© 2020. Published by The Company of Biologists Ltd | Journal of Experimental Biology (2020) 223, jeb217703. doi:10.1242/jeb.217703

RESEARCH ARTICLE

Spectral organization of the compound eye of a migrating nymphalid, the chestnut tiger butterfly *Parantica sita*

Nicolas Nagloo, Michiyo Kinoshita and Kentaro Arikawa*

ABSTRACT

Several butterflies of family Nymphalidae perform long-distance migration. Extensive studies of migration in the iconic monarch butterfly *Danaus plexippus* have revealed that vision plays a crucial role in migratory orientation. Differences in the migratory patterns of butterflies suggest that not all species are exposed to the same visual conditions and yet, little is known about how the visual system varies across migratory species. Here, we used intracellular electrophysiology, dye injection and electron microscopy to assess the spectral and polarization properties of the photoreceptors of a migrating nymphalid, *Parantica sita*. Our findings reveal three spectral classes of photoreceptors including ultraviolet, blue and green receptors. The green receptor class contains three subclasses, which are broad, narrow and double-peaking green receptors. Ultraviolet and blue receptors are sensitive to polarized light parallel to the dorso-ventral axis of the animal, while the variety of green receptors are sensitive to light polarized at 45 deg, 90 deg and 135 deg away from the dorso-ventral axis. The polarization sensitivity ratio is constant across spectral receptor classes at around 1.8. Although *P. sita* has a typical nymphalid eye with three classes of spectral receptors, subtle differences exist among the eyes of migratory nymphalids, which may be genus specific.

KEY WORDS: Photoreceptor, Vision, Insect, Migration, Spectral sensitivity

INTRODUCTION

The visual system of butterflies is diverse and complex, which is apparent in the compound eye photoreceptors. Despite evolving from trichromats with ultraviolet (UV), blue (B) and green (G) photoreceptors, butterflies have developed spectrally diverse photoreceptors most likely for color vision (Briscoe and Chittka, 2001; Marshall and Arikawa, 2014). Color vision is best studied in the Japanese yellow swallowtail *Papilio xuthus*. The eyes of *P. xuthus* are furnished with at least 6 classes of spectral (photo)receptors, which are UV, violet (V), B, G, red (R) and broadband (BB) sensitive. Their excellent color vision is a tetrachromatic system based on the UV, B, G and R receptors (Koshitaka et al., 2008).

Accumulated evidence has suggested that this diversity of butterfly photoreceptors seems genus-specific with variations observed within butterfly families (Stavenga et al., 2001; Wakakuwa et al., 2007). The diversity of *P. xuthus* photoreceptors is created by the combination of filtering effects of colored and fluorescent screening pigments and the expression of multiple opsins in some photoreceptors (Arikawa, 2003). Papilionid species of the genus *Graphium* seem to have eyes of even richer spectral variety: the common blue bottle *Graphium sarpedon* has at least 15 distinct spectral receptors (Chen et al., 2016). Similar mechanisms create photoreceptor polymorphism in the family Pieridae: the cabbage white *Pieris rapae* has two spectrally distinct red receptors (Stavenga and Arikawa, 2011), while the pale clouded yellow *Colias erate* has three spectrally distinct red-sensitive photoreceptors only in females (Ogawa et al., 2013). Although the family Nymphalidae generally has simpler eyes compared with other families, photoreceptor complements still range from simple to complex, especially when comparing species such as the small tortoiseshell *Aglais urticae* (Steiner et al., 1987) and the red postman *Heliconius erato* (McCulloch et al., 2016).

Several nymphalid species including the monarch (*Danaus plexippus*), red admiral (*Vanessa atalanta*) and painted lady (*Vanessa cardui*) are known for achieving long-distance migration (Stefanescu, 2001; Stefanescu et al., 2007; Urquhart and Urquhart, 1978). Among these, *D. plexippus* is the model species for the study of visual systems and visual orientation during migration (Blackiston et al., 2011; Sauman et al., 2005; Stalleicken et al., 2006). UV-, B- and G-absorbing visual pigments are expressed in the eye of *D. plexippus* in three fixed combinations, providing the basis of the photoreceptor spectral sensitivities (SS) peaking at the UV, B and G wavelength regions. However, in the dorsal rim area, photoreceptors are only sensitive to UV and have a specialized rhabdom structure that provides enhanced polarization sensitivity (PS). Orientation seems to be a multi-sensory process, depending on the UV polarization cues and the time-compensated compass mechanism (Merlin et al., 2009; Reppert et al., 2004; Sauman et al., 2005).

The chestnut tiger butterfly *Parantica sita* is another famous nymphalid, which migrates more than 2400 km between central Japan and Hong Kong (Kanazawa et al., 2015). Although *P. sita* and *D. plexippus* both perform long-distance migration, there are differences between their migratory patterns. Unlike *D. plexippus*, *P. sita* has part of its migratory route over the ocean, providing them with very different light conditions and landscapes for orientation. Furthermore, *P. sita* migrates south and north in one generation for each leg of its migratory journey (Miyatake et al., 2003; Yu, 2011). In contrast, *D. plexippus* individuals travel south in a single generation but take approximately five generations to complete their northbound journey (Urquhart and Urquhart, 1978). Variations in migratory patterns suggest that there may be differences across the visual systems among migratory butterflies.

Here, we have started to characterize the visual system of *P. sita*. We studied the spectral and polarization properties of photoreceptors by intracellular electrophysiological recordings

Laboratory of Neuroethology, SOKENDAI (The Graduate University for Advanced studies), Hayama 240-0193, Japan.

*Author for correspondence (arikawa@soken.ac.jp)

N.N., 0000-0002-6564-5737; M.K., 0000-0002-5818-9622; K.A., 0000-0002-4365-0762

Received 29 October 2019; Accepted 30 December 2019

Journal of Experimental Biology (2020) 223, jeb217703. doi:10.1242/jeb.217703

coupled with dye injection to localize them within the ommatidium. We also studied the ommatidial ultrastructure by transmission electron microscopy, and discuss our findings in comparison with other butterflies, particularly with nymphalid species.

MATERIALS AND METHODS

Animal specimens

We collected adults of the chestnut tiger butterfly *Parantica sita niphonica* in Narusawa Village in Yamanashi prefecture in August and September, and on Kikaijima Island in Kagoshima prefecture. We also used individuals caught in Hinomisaki (Wakayama prefecture), Murotomisaki (Kochi prefecture), Onoda City (Yamaguchi prefecture) and Ishima Island (Tokushima). In total, we used 90 males and 32 females.

Intracellular recordings

Butterflies were mounted on a custom-made stage and held in place with beeswax to reduce movement during the electrophysiological recordings. The mounted specimen was placed at the center of the Cardan arm perimeter device set in a Faraday cage. Chloridized silver wire placed in the stump of an antenna served as the reference electrode. Active electrodes were made using borosilicate glass tubes with an outer diameter of 1 mm and an inner diameter of 0.5 mm and pulled in a P-1000 Flaming/Brown micropipette puller (Sutter, USA). The glass micropipettes were then filled with 3 mol l^{-1} potassium chloride and had a resistance of 60–80 MΩ. A small triangular cut was made at the corneal surface through which the glass electrode was inserted into the retina. The active electrode was moved deeper into the eye using a PM 10 piezo manipulator (Märzhäuser, Germany) to penetrate single photoreceptor cells and enable intracellular recordings of electrical responses to light stimuli.

Spectral and polarization sensitivities

A 500 W xenon lamp was used as the light source and the light passed through a series of 23 interference filters ranging from 300 nm to 740 nm at 20 nm intervals. The light was led into the Faraday cage through a quartz optic fiber whose end was fixed on the arm of the perimeter device. The photon fluxes of all monochromatic lights were measured with a Model-470D radiometer (Sanso, Tokyo) and were adjusted to be isoquantal using a neutral density wheel. After locating the optical axis of the penetrated photoreceptor, monochromatic lights were flashed from short to long wavelengths and in reverse order for a stimulation duration of 30 ms at 1 s intervals. The monochromatic light that produced the maximal response was passed through a UV-transparent rotating polarization filter to measure the cell's polarization sensitivity (PS). The polarization (*e*-vector) angle parallel to the animal's dorso-ventral axis was defined as 0 deg. During each measurement, a full 360 deg rotation is performed with measures taken at 10 deg intervals. This produced two consecutive measures of PS with 18 data points each. PS is often summarized as a ratio between the maximum and minimum sensitivities known as the PS ratio. In this case, the peak sensitivity and minimum sensitivity were calculated as an average across 5 data points centered on the peak and minima, respectively, and then dividing the average peak sensitivity by the average minimum sensitivity to obtain the PS ratio. For each recording, the cell was stimulated with lights of varying intensity over 5–6 log units to record a response voltage–log stimulus intensity (V–log I) function, which allowed us to convert responses into sensitivities. Only recordings with a maximum voltage above 30 mV were selected for further analysis.

K-means clustering of spectral sensitivity functions

To determine the number of spectral receptor classes in *P. sita*, we used a *K*-means clustering algorithm. The Euclidean distance between SS curves was used to assess shape similarity between curves. A cluster was formed by randomly selecting a SS curve to act as an initial centroid. All curves were assigned to the most similar initial centroid, which was then updated to the average of all curves clustered to the initial one. The similarity between centroids and curves was checked throughout multiple iterations and each time, curves were sent to the most similar group and the centroid updated until the centroid no longer changed. For each cluster, this process was replicated with 1000 random initializations to ensure that the best fitting clusters could be detected as results were affected by the selection of the initial centroid. A similarity score was derived from the Euclidean distance between clusters and centroids where a score of 1 is the equivalent of a perfect match. With every additional cluster, the overall fit between curves and centroids improved. However, the rate of improvement flattened out once the optimal number of clusters had been exceeded. The number of clusters prior to the flattening indicated the optimal number of spectral receptor classes of *P. sita*.

Visual pigment template fitting

For each spectral receptor class derived from the *K*-means algorithm, we calculated the best-fitting visual pigment absorption spectrum based on the Govardovskii template (Govardovskii et al., 2000). We assumed that opsins were bound to 11-*cis*-3-hydroxyretinal as in other lepidopteran species (Seki et al., 1987), which offers a good approximation of the variation of the SS curves of invertebrate visual pigments (Stavenga, 2010). Only data points after 80% of the peak on the short-wavelength side of the final averaged SS curve were used to identify the best fit. Visual pigments were re-iteratively fitted to the data points until the visual pigment with the smallest root mean square error was found.

Dye-injection experiments

Lucifer Yellow was used to visualize cells after electrical recordings. Electrode tips were filled with 2.5% Lucifer Yellow in 0.1 mol l^{-1} lithium chloride and back filled with 3 mol l^{-1} lithium chloride. Once the electrical responses of a cell were recorded, a negative 3 nA DC current was passed through the electrode for 2–3 min. The eye was then dissected out of the head capsule, fixed in 4% paraformaldehyde in 0.1 mol l^{-1} cacodylate buffer for 1 h, and dehydrated through a series of ascending acetone concentrations. The tissue was then infiltrated with propylene oxide and embedded in Epon 812. Embedded tissue samples were sectioned at 10 µm thickness using a rotary microtome (Microm HM 355S, ThermoFisher, USA) and the Lucifer Yellow-filled cells were visualized under blue–violet excitation light using an epi-fluorescence microscope (Olympus BX-60, Tokyo, Japan).

Electron microscopy

For conventional transmission electron microscopy, eyes were dissected from the head capsule and pre-fixed in 2.5% glutaraldehyde (GA) and 2% paraformaldehyde (PA) in 0.1 mol l^{-1} cacodylate buffer (pH 7.3, CB) overnight. The eyes were then post-fixed in 2% osmium tetroxide (OsO_4) in 0.1 mol l^{-1} CB for 2 h at room temperature before being stained with 2% uranyl acetate in 50% ethanol for 1 h. After dehydration in an ethanol series, the eyes were embedded in Spurr's resin. Ultrathin sections stained with uranyl acetate and lead citrate were observed in a transmission electron microscope (H7650, Hitachi, Japan).

Journal of Experimental Biology (2020) 223, jeb217703. doi:10.1242/jeb.217703

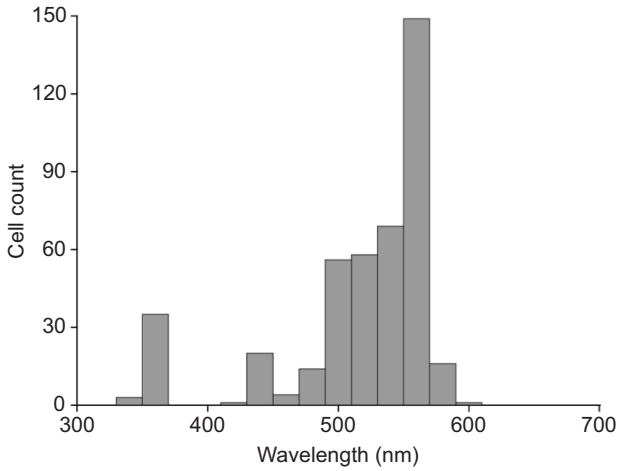

Fig. 1. Distribution of peak spectral sensitivity in the migratory chestnut tiger butterfly *Parantica sita*. Distribution of wavelength of peak sensitivity across all recorded photoreceptors. Bin width=20 nm. *N*=122/401 butterflies/photoreceptors.

We also obtained serial EM images of part of the eye containing 18 ommatidia by using a serial block face-scanning electron microscope (SBF-SEM) (Zeiss Gemini 300 equipped with Gatan 3view2, Germany). For SBF-SEM, eyes were pre-fixed with 4% GA plus 1% PA in 0.15 mol l^{-1} CB with 2 mmol l^{-1} $CaCl_2$ (CB-Ca) overnight. The eyes were then post-fixed in 2% OsO_4 plus 1.5% K-ferrocyanide in CB-Ca on ice for 1 h. After incubation in 1% aqueous solution of thiocarbohydrazide for 20 min, the eyes were again post-fixed with 2% aqueous OsO_4 for 30 min at room temperature, and then block-stained in 1% aqueous uranyl acetate at 4°C overnight. On the next day, the tissues were block-stained with Walton's lead aspartate solution for 30 min at 60°C, dehydrated with a graded series of ethanol and embedded in hard Spurr's resin (Deerinck et al., 2010). Serial images were collected every 1 µm at a cutting angle perpendicular to the ommatidial optical axis. The size of the rhabdomeres was measured using ImageJ/TrakEM2 software (Cardona et al., 2012).

RESULTS

We analyzed 401 photoreceptors in total. The peaks of their SS curves (λ_{max}) ranged from 350 nm to 600 nm with a trimodal distribution: cell counts peaking at 360, 440 and 560 nm (±10 nm, Fig. 1).

Using the *K*-mean algorithm, we analyzed the similarity of SS curves to each other to determine the number of spectral receptor classes. As the number of clusters (K) used to explain the distribution of SS is increased, the fit between clusters and the dataset improves and a greater similarity score is achieved (Fig. 2A). After the fifth cluster, additional clusters provide minimal improvement of fit (<10% of maximum improvement),

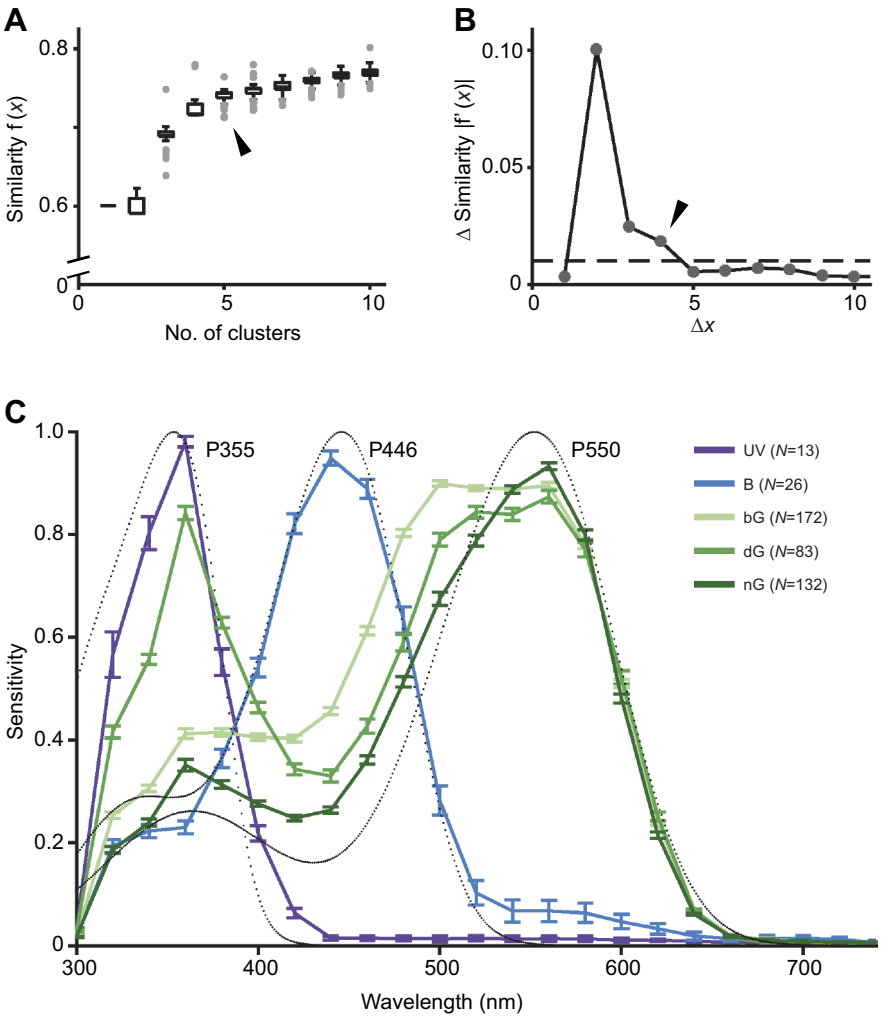

Fig. 2. Clustering photoreceptor classes by the similarity of the shape of their spectral sensitivity curves. (A) Median within-cluster similarity scores over 1000 replicates across clusters for 1–10 clusters. (B) Change in similarity score as the number of clusters increases. The dashed line indicates the threshold after which additional clusters provide less than 10% of the peak improvement in similarity between clusters and dataset. (C) Spectral sensitivity curves of the five classes obtained from the *K*-means algorithm. Dotted lines illustrate the absorption spectra of visual pigment with A1 chromophore (Govardovskii et al., 2000) best fit to the UV, B, bG, dG and nG spectral sensitivities. The black arrowheads in A and B indicate the last point above this threshold, suggesting that five photoreceptor classes are enough to explain the variation in spectral sensitivity of *P. sita* photoreceptors. The dashed line in B indicates the threshold after which additional clusters provide less than 10% of the peak improvement in similarity between clusters and dataset. The error bars in C indicate s.e.m. Photoreceptors: UV, UV-sensitive; B, blue; bG, broad green; dG, double-peaking green; nG, narrow green.

Journal of Experimental Biology (2020) 223, jeb217703. doi:10.1242/jeb.217703

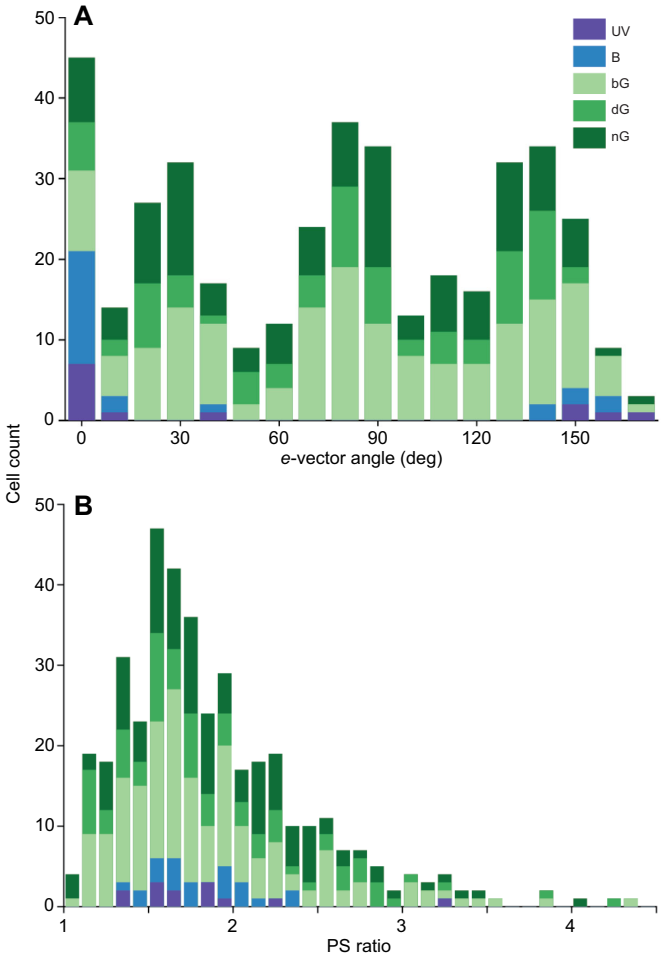

Fig. 3. The polarization sensitivity properties of the five photoreceptor classes. (A) The distribution of *e*-vectors of peak sensitivity. (B) Distribution of the polarization sensitivity (PS) ratio.

suggesting that 5 photoreceptor types are sufficient to explain the variation in the SS of measured photoreceptors (Fig. 2B).

Table 1. Polarization sensitivity (PS) ratio of photoreceptor classes

Photoreceptor class	PS ratio	s.d.	Count
UV	1.81	0.51	13
B	1.81	0.28	23
bG	1.85	0.58	165
dG at 560 nm	1.92	0.64	80
dG at 360 nm	1.23	0.17	12
nG	1.91	0.54	120

The λ_{max} of the five spectral receptor classes occur at 360 nm, 440 nm and 560 nm (Fig. 2C) matching the trimodal distribution of λ_{max} across all recordings (Fig. 1). The receptors can be identified as UV, B, broad green (bG), double-peaking green (dG) and narrow green (nG) (Fig. 2C). Although bG, dG and nG have been identified as separate subclasses, a high similarity in their λ_{max} and the long-wavelength limb of their SS curves is evident. Fitting single visual pigment templates to the SS curves revealed that UV, B and G receptors can be reasonably explained by visual pigments absorbing maximally at 355 nm, 446 nm and 550 nm (P355, P446 and P550), respectively.

The PS measurements revealed that UV and B receptors are mainly sensitive to vertically polarized light (0 deg), while the G class receptors are sensitive to a broader range of *e*-vector angles peaking at 45 deg, 90 deg and 135 deg (Fig. 3A). We measured the PS ratio of the receptors at their peak wavelengths of SS: for the dG receptor, the PS was measured also at its secondary peak at 360 nm. The PS ratio across all cells ranged from 1 to 5 with the peak at 1.5 to 2 (Fig. 3B), but the average values appeared constant around 1.8 among all classes (Table 1).

We located the optical axis of recorded photoreceptors by moving the Cardan arm perimeter device until maximal responses were observed. The position of the animal in the center of rotation of the perimeter device allowed us to locate the ommatidia housing each recorded photoreceptor in the compound eye. The recorded ommatidia were clustered around the mid-anterior region of the eye (Fig. 4). The vertical spread of measurements spanned about 120 deg, with the most dorsal measurement located 70 deg above the equator and the lowest 45 deg below. The horizontal spread was slightly smaller with a span of about 100 deg with the most posterior measurement occurring 35 deg behind the midpoint of the eye and

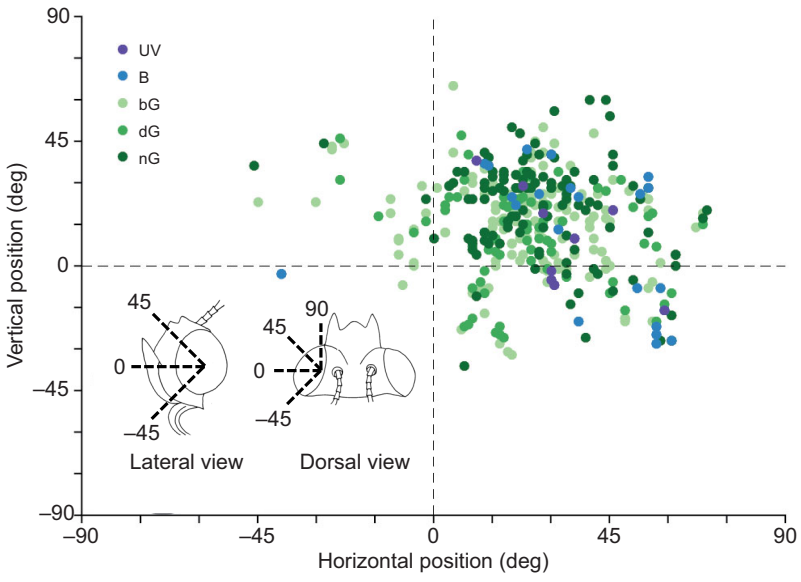

Fig. 4. Angular position of the different classes of photoreceptors recorded in the compound eye of *P. sita*. The inset shows the lateral and dorsal view of the head of *P. sita* with illustrations of angles (in deg).

Journal of Experimental Biology (2020) 223, jeb217703. doi:10.1242/jeb.217703

the most anterior 65 deg in front. No noticeable difference in the spatial distribution of spectral receptors was observed in this area of the compound eye (Fig. 4).

We injected Lucifer Yellow into the recorded photoreceptors to localize them in the ommatidium (Fig. 5). Each ommatidium contains nine photoreceptor cells R1–R9 (see Fig. 6) as in other butterfly species (Wakakuwa et al., 2007). Dye injection revealed that the UV and B receptors are R1 and R2, while the G class receptors are R5–R8 also as observed in other butterflies. No information was obtained for R9 receptors.

To correlate the electrophysiological results with the cells' precise anatomy, we observed the rhabdom ultrastructure in the mid-anterior region of the eye. The conventional TEM confirms that the rhabdom, 2–3 µm in diameter and about 500 µm in length, is

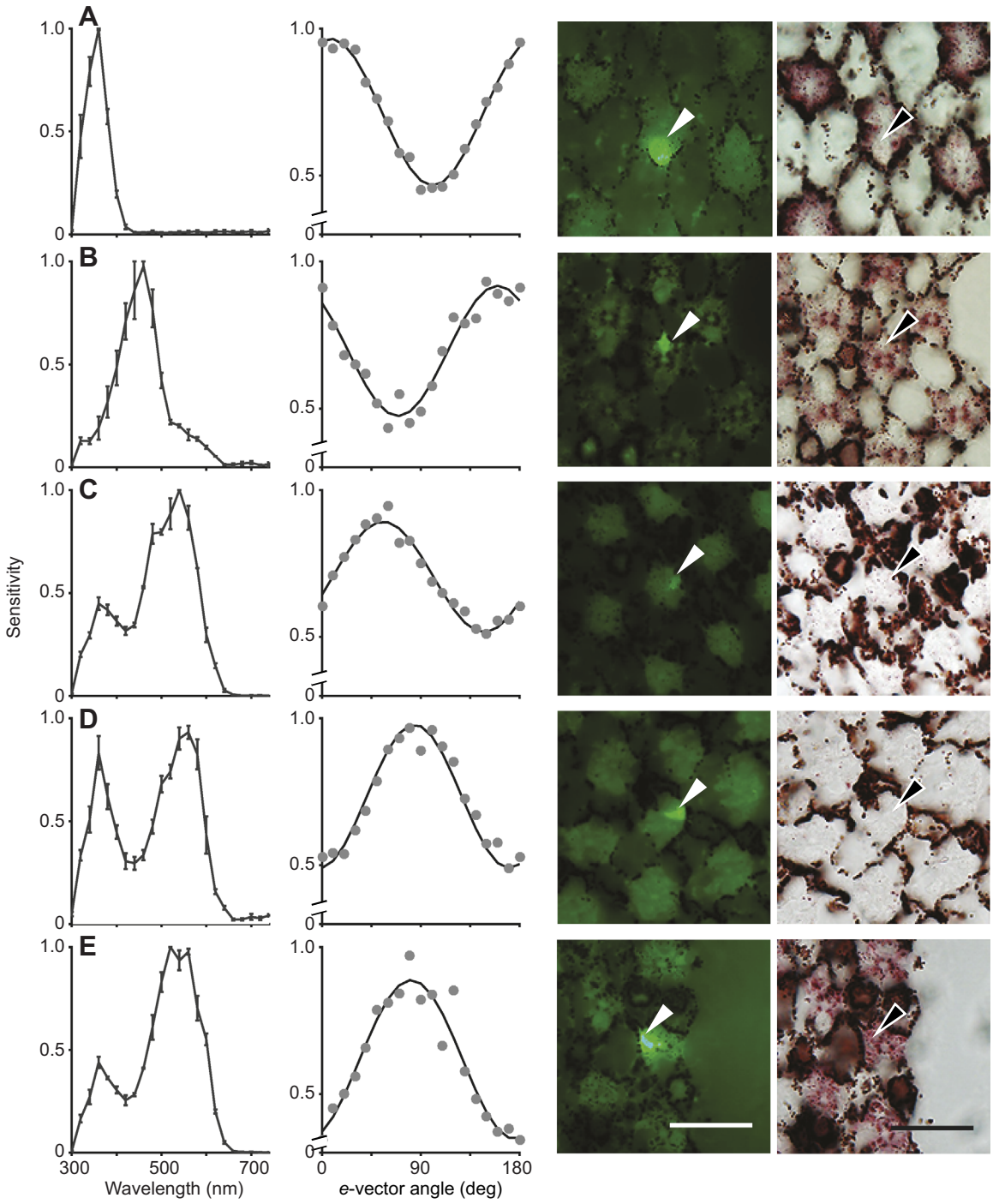

Fig. 5. Spectral sensitivity, polarization sensitivity and dye-injected images of *P. sita* photoreceptors. Spectral sensitivity (right), polarization sensitivity (second column) and micrographs (left) of (A) UV, (B) blue, (C) broad green, (D) double-peaking green and (E) narrow green receptors. Arrowheads indicate cells stained with Lucifer Yellow in fluorescence and conventional microscopy. Sections were obtained at various depths: B and C are from the distal region where dense reddish pigment surrounds the rhabdom in all ommatidia. All images are oriented so that the dorsal side of the animal is towards the top of the page. Scale bars: 20 µm.

Journal of Experimental Biology (2020) 223, jeb217703. doi:10.1242/jeb.217703

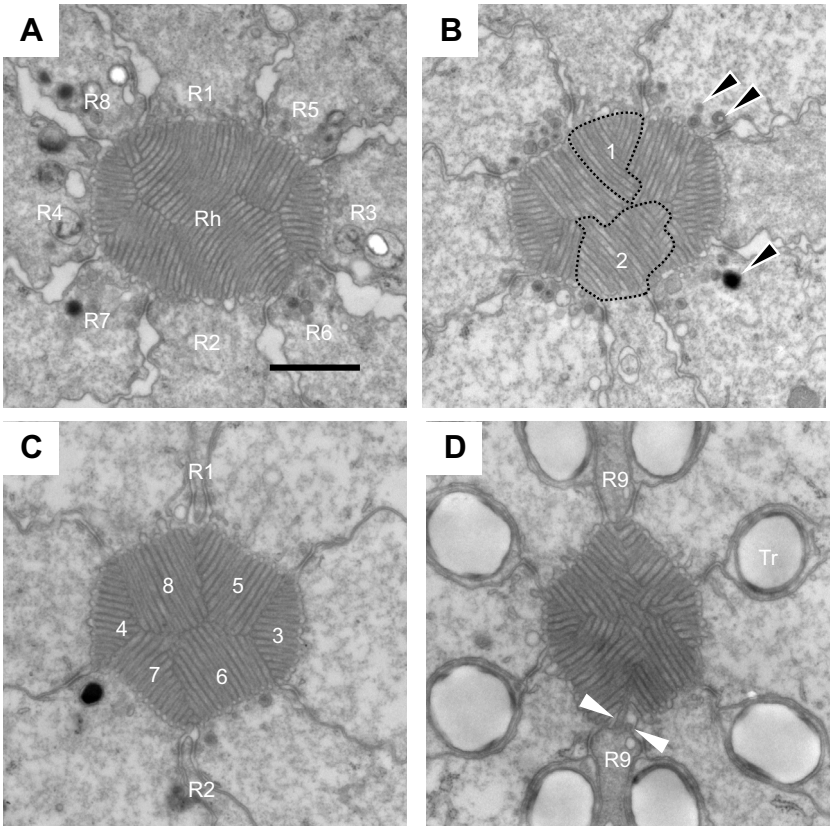

Fig. 6. Rhabdom ultrastructure of the ommatidia of the mid-anterior region of the eye of *P. sita*. (A) Distal region where R1–R8 photoreceptors contribute their microvilli to form the rhabdom (Rh) in the center. (B) Middle region where the rhabdomeres of R1 and R2 photoreceptors (1 and 2) are marked. Black arrowheads indicate pigment granules. (C) Proximal region where R1 and R2 have no microvilli. Numbers 3–8 indicate the rhabdomeres of R3–R8 photoreceptors. (D) Basal region where the bilobed R9 photoreceptor extend a few microvilli (white arrowheads) towards the rhabdom. Tr, tracheole that coalesces at the ommatidial base to form the tapetal mirror. Scale bar: 1 µm.

composed of rhabdomeres of R1–R9 photoreceptor cells. The rhabdomeral microvilli of R1 and R2 are parallel but alternately curve into two directions at 45 deg and 135 deg depending on the depth (Fig. 6A,B), making the main orientation of the microvilli in mass parallel to the animal's dorso-ventral axis (=0 deg). In contrast, R3–R8 contribute straight and parallel microvilli in the entire length of the rhabdom. R3 and R4 are aligned to the antero-posterior (=90 deg) axis of the animal, while R5 and R7, and R6 and R8 are paired along the two main diagonal axes (Fig. 6C). Close to the base of the ommatidium, R9 can be observed as a bilobed cell contributing a few straight microvilli at 0 deg (Fig. 6D).

We measured cross-sectional area of each rhabdomere in seven neighboring ommatidia in an image stack obtained by SBF-SEM (Fig. 7A). R1 and R2 rhabdomeres ended at depths of either 300 µm (short; S) or 400 µm (long; L) from the rhabdom tip. The combination of S and L rhabdomeres between R1/R2 revealed three ommatidial types across the seven measured ommatidia: L/S or S/L (n=4), S/S (n=2), L/L (n=1). (Fig. 7B)

DISCUSSION

Ommatidial heterogeneity and photoreceptor diversity

The ommatidium of *Parantica sita* has a more or less cylindrical rhabdom where all the nine ommatidial photoreceptors R1-R9 contribute their rhabdomeral microvilli (Fig. 6). The SBF-SEM analysis has revealed that the rhabdom of *P. sita* is partially tiered. The R1 and R2 dominate the rhabdom only in its distal half or so, while R3–R8 have microvilli in the entire length of the rhabdom. The variable length of the R1 and R2 rhabdomeres indicate three types of ommatidia (Fig. 7B), presumably corresponding to spectrally distinct ommatidia in other butterfly species (Wakakuwa et al., 2007) including the monarch *D. plexippus* (Sauman et al., 2005).

In the L/S (or S/L) type ommatidia, the cross-sectional area of the short rhabdomeres is larger distally (Fig. 7B). Such a depth-dependent size difference of R1 and R2 rhabdomeres has been observed also in the small white *Pieris rapae* (Qiu et al., 2002). There, the photoreceptors with larger rhabdomeres in the distal tip are UV sensitive, and those with smaller rhabdomeres are blue sensitive (Qiu and Arikawa, 2003). This matches the general arrangement of spectral receptors in an ommatidium: shorter wavelength receptors tend to have larger rhabdomeres in more distal regions of the rhabdom (Matsushita et al., 2012). Presumably, the photoreceptors with short rhabdomeres are UV sensitive, while those with long rhabdomeres are blue sensitive in *P. sita*.

The dye injection and PS measurement results support the assumption that UV and B receptors are either R1 or R2, and that G class receptors are R3–R8. The spectral sensitivities of the distally situated UV and B receptors match well with the absorption spectra of visual pigments peaking at 355 nm (P355) and 456 nm (P456), respectively. This suggests that the self- and lateral-screening effects among rhabdomeres (Snyder et al., 1973) are negligible here (Fig. 2C). In contrast, the G class receptors exhibit a large variation on the short-wavelength side of the SS curves. *K*-means clustering has revealed three possible stable subclasses of G receptors with variations represented by the standard error bars. Similar variation in the SS of G receptors has been reported in the Asian comma butterfly *Polygonia c-aurem* and the great purple emperor *Sasakia charonda* (Kinoshita et al., 1997). The long-wavelength limb of *P. sita* G receptors matches the absorption spectrum of a visual pigment with maximal absorbance at 550 nm (P550) (Fig. 2C) and is almost identical across all three G receptors. Although not specified at this stage, the variations are most likely attributable to some filtering effects of neighboring rhabdomeres (Snyder et al., 1973), tiered organization of the rhabdom and some photostable

Journal of Experimental Biology (2020) 223, jeb217703. doi:10.1242/jeb.217703

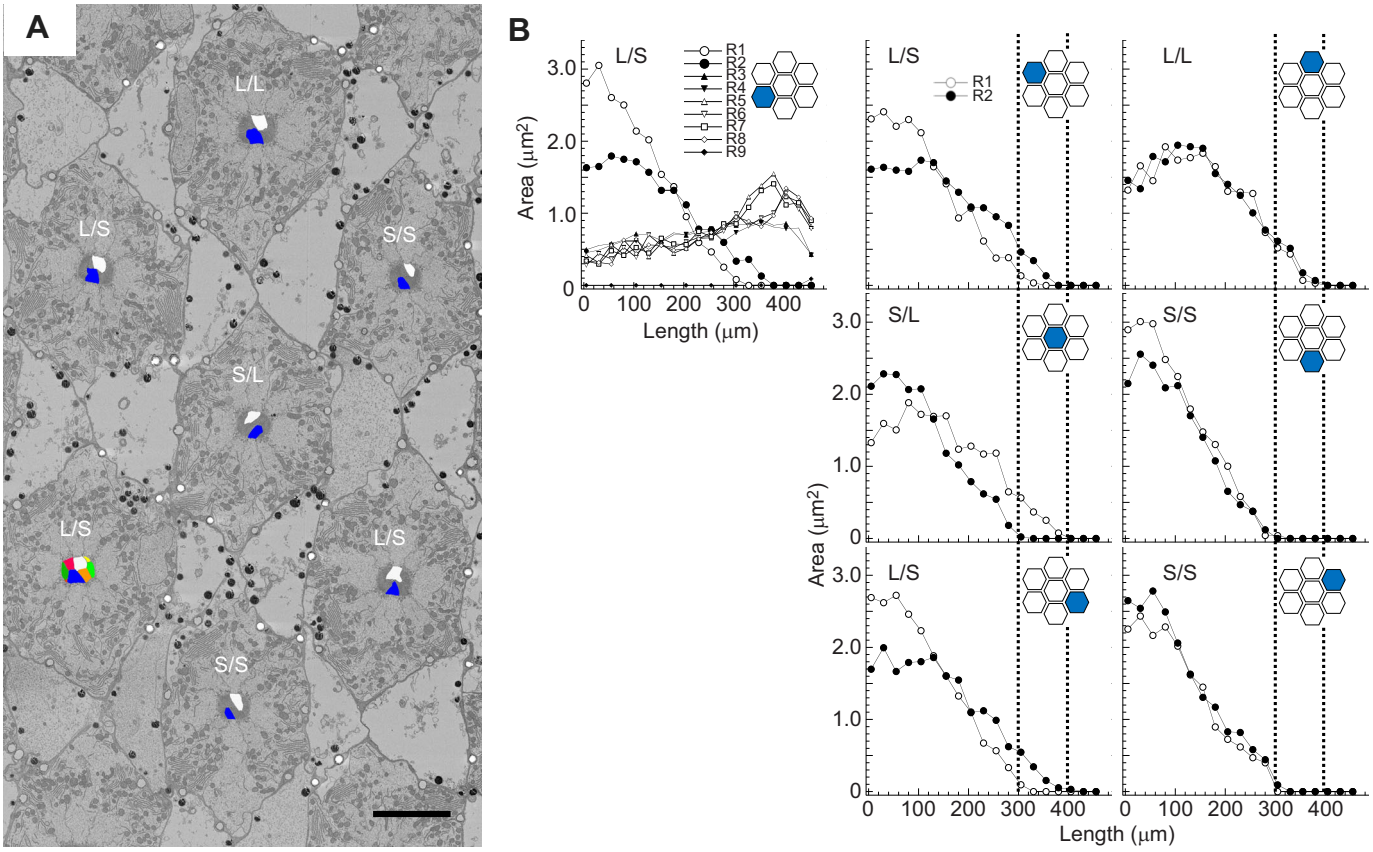

Fig. 7. Ommatidial heterogeneity revealed by serial block face-scanning electron microscopy (SBF-SEM). (A) An image from the SBF-SEM stack at the depth of about 240 µm from the distal tip of the rhabdom. The rhabdomeres whose areas were measured were painted. L/L, long/long; S/S, short/short; L/S (S/L), long/short (short/long). Scale bar: 10 µm. (B) Rhabdom areas plotted against the rhabdom depth. The hexagonal pattern in each graph shows the position of the particular ommatidium in the EM image in A.

screening pigments (Stavenga and Arikawa, 2011). In fact, the *P. sita* photoreceptors contain at least two kinds of pigment granules around the rhabdom (Fig. 6B), which are most likely acting as spectral filters by absorbing the boundary wave of the light propagating in the rhabdom (Stavenga and Arikawa, 2011). Additional molecular biological and anatomical experiments are necessary to fully comprehend the observed G receptor variations.

Comparative aspects

The UV, B and G receptors of *P. sita* most likely express the visual pigments P365, P446 and P550, respectively. The trichromatic expression pattern appears common in nymphalids, including those that perform long-distance migration (Briscoe and Bernard, 2005; Briscoe et al., 2003): exceptions are *Heliconius* species, which have two distinct UV opsins (Briscoe et al., 2010; McCulloch et al., 2016). The visual pigment molecules of nymphalids are highly homologous, suggesting that opsin expression is conserved across migrating nymphalids (Sauman et al., 2005). Despite this, the λ_{max} of the B and G receptors are long wavelength shifted in *P. sita* (446 nm and 550 nm) compared with *D. plexippus* (435 nm and 545 nm) (Stalleicken et al., 2006), reflecting subtle differences in the visual system of these two species. In fact, the 550 nm peak is the second longest among G receptors of nymphalids following 580 nm of *P. c-aureum* (Kinoshita et al., 1997). It would be particularly interesting to investigate whether or not this difference has been created through positive selection, as seen in *Limenitis* species (Frentiu et al., 2007).

We measured photoreceptor PS to localize them in the ommatidium based on the orientation of the rhabdomeral microvilli (Arikawa and Uchiyama, 1996; Bandai et al., 1992; Lin, 1993; Moody and Parriss, 1961). In general, photoreceptors with short rhabdomeres are reported to exhibit higher PS ratios than those with longer rhabdomeres (Snyder, 1973). Here, we found in *P. sita* that an average PS ratio of 1.8 is maintained across all spectral receptor classes (Table 1). The rhabdomeres of R1 and R2 are shorter than those of R3–R8, but their microvilli are curved with oscillating orientation, which probably suppresses their PS (Fig. 6B,C). Similar rhabdomeric configuration is found in a number of butterflies (Arikawa et al., 1999; Gordon, 1977; Kolb, 1978; Qiu et al., 2002). This is probably a widely employed strategy to reduce PS of selected photoreceptors similar to the rhabdom twist observed in bee photoreceptors (Menzel and Snyder, 1974; Wehner et al., 1975). In fact, the UV- and blue-sensitive R1 and R2 of *Pieris rapae* have virtually no PS because of the curved rhabdomeral microvilli (Blake et al., 2019). Still, *P. sita*, as well as *D. plexippus* (Reppert et al., 2004; Stalleicken et al., 2006), retains a set of photoreceptors sensitive to vertical, horizontal and diagonal polarization in the main part of the eye. The PS ratio of *D. plexippus* photoreceptors appears to be slightly higher (PS=∼2.8) than the value PS=∼1.8 of *P. sita* (Reppert et al., 2004; Stalleicken et al., 2006), although the significance of this difference needs further study. A set of polarization-sensitive photoreceptors would provide the physiological basis for some degree of polarization vision, if any, as in *Papilio* butterflies (Kelber, 1999; Kinoshita et al., 2011; Stewart et al., 2019).

We found a correlation of SS and PS of photoreceptors in *P. sita*: UV and B receptors are sensitive to vertically (0 deg) polarized light, while G receptors are sensitive to 45 deg, 90 deg and 135 deg polarized light. This correlation is well conserved across butterflies (Bandai et al., 1992; Blake et al., 2019; Kinoshita et al., 1997), which has given rise to polarization-dependent color vision in *Papilio*. This combined visual capacity appears to function as a 'matched filter' for ovipositing females to find the best leaf on which to lay eggs based on the angle and color of the leaf (Kelber, 1999; Kelber et al., 2001). It would not be surprising if *P. sita* uses such a combined capacity to create matched filters in some specific behavioral context.

The anatomy of *P. sita* eyes (Figs 6 and 7) is of a rather simple nymphalid type (Gordon, 1977). This study provides clear evidence that their eyes are furnished with the basic set of UV, B and G receptors. The observed polymorphism of G receptors of *P. sita* is more like *P. c-aureum*, a non-migrating flower feeder (Kinoshita et al., 1997) than the migrating *D. plexippus* (Stalleicken et al., 2006). This may reflect possible difference in their feeding behaviors.

There is still a possibility that *P. sita* also has red-sensitive photoreceptors. This is because the epi-illumination microscopy of *P. sita* has revealed that small numbers of ommatidia have dark red tapetal reflection among the majority of yellow-reflecting ommatidia as in other *Parantica* species (Stavenga et al., 2001). The dark red tapetal reflection is due to dense red perirhabdomal pigment, which makes P560-expressing photoreceptors into dark red receptors peaking at 640 nm in the eye of *Pieris rapae* (Stavenga and Arikawa, 2011). However, we did not encounter photoreceptors with the peak wavelength longer than 560 nm in the present study. Such receptors perhaps occur more in the ventral eye region where *P. sita* see objects on the ground, such as nectar providing flowers. Or, these receptors may be the small basal R9 photoreceptors that had little chance to be penetrated. The red-reflecting ommatidia are absent in *V. cardui* and *V. atalanta* that have only three classes of spectral receptors (Briscoe et al., 2003; Zaccardi et al., 2006), but probably exist in *D. plexippus* (Miller and Bernard, 1968; Stavenga et al., 2001). This suggests that differences in the photoreceptor complement available to different migratory nymphalids are phylogenetically influenced.

Whether and how *P. sita* also uses polarized light cues and a sun compass to orient itself would also be of particular interest. If this is the case, it would be necessary to investigate the dorsal rim area to determine whether the neural basis for this behavior is similar to *D. plexippus*. Differences in the onset of the migratory mode between *P. sita* and *D. plexippus* will also allow us to further dissect the formation of the neural circuits responsible for visual orientation during migration in *P. sita*.

Acknowledgements
We thank Mr Itaru Kanazawa and Mr Makoto Fukushima, for discussions and help in collecting live *P. sita* specimens in the field. Mr Takumi Fukumura (Onoda), Mr Yutaka Murakami (Ishima Island) and Mr Masahiro Fujino (Murotomisaki) kindly sent live specimens to the laboratory. Our special thanks also go to the Chestnut Tiger Research Group for inviting one of us (M.K.) to introduce our work on the Chestnut Tiger vision in an annual meeting.

Competing interests
The authors declare no competing or financial interests.

Author contributions
Conceptualization: M.K.; Formal analysis: N.N., K.A.; Investigation: N.N., M.K., K.A.; Writing - original draft: N.N.; Writing - review & editing: N.N., M.K., K.A.; Supervision: M.K., K.A.; Funding acquisition: N.N., M.K., K.A.

Funding
This work was supported by the Japanese Society for the Promotion of Science (JSPS) via a post-doctoral fellowship and KAKENHI grant (17F17720 to N.N.) and KAKENHI grants for Scientific Research (17H05973 to M.K. and 18H05273 to K.A.).

References
Arikawa, K. (2003). Spectral organization of the eye of a butterfly, *Papilio*. *J. Comp. Physiol. A* **189**, 791-800. doi:10.1007/s00359-003-0454-7

Arikawa, K. and Uchiyama, H. (1996). Red receptors dominate the proximal tier of the retina in the butterfly *Papilio xuthus*. *J. Comp. Physiol. A* **178**, 55-61. doi:10.1007/BF00189590

Arikawa, K., Scholten, D. G. W., Kinoshita, M. and Stavenga, D. G. (1999). Tuning of photoreceptor spectral sensitivities by red and yellow pigments in the butterfly *Papilio xuthus*. *Zool. Sci.* **16**, 17-24. doi:10.2108/zsj.16.17

Bandai, K., Arikawa, K. and Eguchi, E. (1992). Localization of spectral receptors in the ommatidium of butterfly compound eye determined by polarization sensitivity. *J. Comp. Physiol. A* **171**, 289-297. doi:10.1007/BF00223959

Blackiston, D., Briscoe, A. D. and Weiss, M. R. (2011). Color vision and learning in the monarch butterfly, *Danaus plexippus* (Nymphalidae). *J. Exp. Biol.* **214**, 509-520. doi:10.1242/jeb.048728

Blake, A. J., Pirih, P., Qiu, X., Arikawa, K. and Gries, G. (2019). Compound eyes of the small white butterfly *Pieris rapae* have three distinct classes of red photoreceptors. *J. Comp. Physiol. A* **205**, 553-565. doi:10.1007/s00359-019-01330-8

Briscoe, A. D. and Bernard, G. D. (2005). Eyeshine and spectral tuning of long wavelength-sensitive rhodopsins: no evidence for red-sensitive photoreceptors among five Nymphalini butterfly species. *J. Exp. Biol.* **208**, 687-696. doi:10.1242/jeb.01453

Briscoe, A. D. and Chittka, L. (2001). The evolution of color vision in insects. *Ann. Rev. Entomol.* **46**, 471-510. doi:10.1146/annurev.ento.46.1.471

Briscoe, A. D., Bernard, G. D., Szeto, A. S., Nagy, L. M. and White, R. H. (2003). Not all butterfly eyes are created equal: rhodopsin absorption spectra, molecular identification and localization of UV- blue- and green-sensitive rhodopsin-encoding mRNA in the retina of *Vanessa cardui*. *J. Comp. Neurol.* **458**, 334-349. doi:10.1002/cne.10582

Briscoe, A. D., Bybee, S. M., Bernard, G. D., Yuan, F., Sison-Mangus, M. P., Reed, R. D., Warren, A. D., Llorente-Bousquets, J. and Chiao, C.-C. (2010). Positive selection of a duplicated UV-sensitive visual pigment coincides with wing pigment evolution in *Heliconius* butterflies. *Proc. Natl. Acad. Sci. USA* **107**, 3628-3633. doi:10.1073/pnas.0910085107

Cardona, A., Saalfeld, S., Schindelin, J., Arganda-Carreras, I., Preibisch, S., Longair, M., Tomancak, P., Hartenstein, V. and Douglas, R. J. (2012). TrakEM2 software for neural circuit reconstruction. *PLoS ONE* **7**, e38011. doi:10.1371/journal.pone.0038011

Chen, P.-J., Awata, H., Matsushita, A., Yang, E.-C. and Arikawa, K. (2016). Extreme spectral richness in the eye of the common bluebottle butterfly, *Graphium sarpedon*. *Front. Ecol. Evol.* **4**, 1-12. doi:10.3389/fevo.2016.00018

Deerinck, T. J., Bushong, E. A., Thor, A. Ellisman, M. H. (2010). NCMIR methods for 3D EM: a new protocol for preparation of biological specimens for serial block face scanning electron microscopy. In *Microscopy and Microanalysis Meeting*, pp. 6-8. Portland, OR, Microscopy Society of America.

Frentiu, F. D., Bernard, G. D., Cuevas, C. I., Sison-Mangus, M. P., Prudic, K. L. and Briscoe, A. D. (2007). Adaptive evolution of color vision as seen through the eyes of butterflies. *Proc. Natl. Acad. Sci. USA* **104**, 8634-8640. doi:10.1073/pnas.0701447104

Gordon, W. C. (1977). Microvillar orientation in the retina of the nymphalid butterfly. *Z. Naturforsch.* **32c**, 662-664. doi:10.1515/znc-1977-7-833

Govardovskii, V. I., Fyhrquist, N., Reuter, T., Kuzmin, D. G. and Donner, K. (2000). In search of the visual pigment template. *Vis. Neurosci.* **17**, 509-528. doi:10.1017/S0952523800174036

Kanazawa, I., Cheng, W. W. W., Pun, H. S. F., Sakiyama, Y. and Doi, H. (2015). First migration record of Chestnut Tiger Butterfly, *Parantica sita niphonica* (Moore, 1883) (Lepidoptera: Nymphalidae: Danainae) from Japan to Hong Kong and longest recorded movement by the species. *Pan-Pacific Entomol.* **91**, 91-98. doi:10.3956/2014-91.1.091

Kelber, A. (1999). Why 'false' colours are seen by butterflies. *Nature* **402**, 251. doi:10.1038/46204

Kelber, A., Thunell, C. and Arikawa, K. (2001). Polarisation-dependent colour vision in *Papilio* butterflies. *J. Exp. Biol.* **204**, 2469-2480.

Kinoshita, M., Sato, M. and Arikawa, K. (1997). Spectral receptors of nymphalid butterflies. *Naturwissenschaften* **84**, 199-201. doi:10.1007/s001140050377

Kinoshita, M., Yamazato, K. and Arikawa, K. (2011). Polarization-based brightness discrimination in the foraging butterfly, *Papilio xuthus*. *Phil. Trans. R. Soc. B* **366**, 688-696. doi:10.1098/rstb.2010.0200

Kolb, G. (1978). Zur Rhabdomstruktur des Auges von *Pieris brassicae* L. (Insecta, Lepidoptera). *Zoomorphologie* **91**, 191-200. doi:10.1007/BF00993860

Koshitaka, H., Kinoshita, M., Vorobyev, M. and Arikawa, K. (2008). Tetrachromacy in a butterfly that has eight varieties of spectral receptors. *Proc. Biol. Sci. B* **275**, 947-954. doi:10.1098/rspb.2007.1614

Lin, J.-T. (1993). Identification of photoreceptor locations in the compound eye of *Coccinella septempunctata* Linnaeus (Coleoptera, Coccinellidae). *J. Insect Physiol.* **39**, 555-562. doi:10.1016/0022-1910(93)90037-R
Marshall, J. and Arikawa, K. (2014). Unconventional colour vision. *Curr. Biol.* **24**, R1150-R1154. doi:10.1016/j.cub.2014.10.025
Matsushita, M., Awata, H., Wakakuwa, M., Takemura, S. and Arikawa, K. (2012). Rhabdom evolution in butterflies: insights from the uniquely tiered and heterogeneous ommatidia of the Glacial Apollo butterfly, *Parnassius glacialis*. *Proc. Biol. Sci.* **279**, 3482-3490. doi:10.1098/rspb.2012.0475
McCulloch, K. J., Osorio, D. and Briscoe, A. D. (2016). Sexual dimorphism in the compound eye of *Heliconius erato*: a nymphalid butterfly with at least five spectral classes of photoreceptor. *J. Exp. Biol.* **219**, 2377-2387. doi:10.1242/jeb.136523
Menzel, R. and Snyder, A. W. (1974). Polarised light detection in the bee, *Apis mellifera*. *J. Comp. Physiol. A* **88**, 247-270. doi:10.1007/BF00697958
Merlin, C., Gegear, R. J. and Reppert, S. M. (2009). Antennal circadian clocks coordinate sun compass orientation in migratory monarch butterflies. *Science* **325**, 1700-1704. doi:10.1126/science.1176221
Miller, W. H. and Bernard, G. D. (1968). Butterfly glow. *J. Ultrastruct. Res.* **24**, 286-294. doi:10.1016/S0022-5320(68)90065-8
Miyatake, Y., Fukuda, H. and Kanazawa, I. (2003). *A Migrating Butterfly, the Chestnut Tiger (in Japanese)*. Tokyo: Gekkan Mushi.
Moody, M. F. and Parriss, J. R. (1961). The discrimination of polarized light by *Octopus*: a behavioral and morphological study. *Z. Vergl. Physiol.* **44**, 268-291. doi:10.1007/BF00298356
Ogawa, Y., Kinoshita, M., Stavenga, D. G. and Arikawa, K. (2013). Sex-specific retinal pigmentation results in sexually dimorphic long-wavelength-sensitive photoreceptors in the Eastern Pale Clouded Yellow butterfly, *Colias erate*. *J. Exp. Biol.* **216**, 1916-1923. doi:10.1242/jeb.083485
Qiu, X. and Arikawa, K. (2003). The photoreceptor localization confirms the spectral heterogeneity of ommatidia in the male small white butterfly, *Pieris rapae crucivora*. *J. Comp. Physiol. A* **189**, 81-88. doi:10.1007/s00359-002-0380-0
Qiu, X., Vanhoutte, K. A., Stavenga, D. G. and Arikawa, K. (2002). Ommatidial heterogeneity in the compound eye of the male small white butterfly, *Pieris rapae crucivora*. *Cell Tissue Res.* **307**, 371-379. doi:10.1007/s00441-002-0517-z
Reppert, S. M., Zhu, H. and White, R. H. (2004). Polarized light helps monarch butterflies navigate. *Curr. Biol.* **14**, 155-158. doi:10.1016/j.cub.2003.12.034
Sauman, I., Briscoe, A. D., Zhu, H., Shi, D., Froy, O., Stalleicken, J., Yuan, Q., Casselman, A. and Reppert, S. M. (2005). Connecting the navigational clock to sun compass input in monarch butterfly brain. *Neuron* **46**, 457-467. doi:10.1016/j.neuron.2005.03.014
Seki, T., Fujishita, S., Ito, M., Matsuoka, N. and Tsukida, K. (1987). Retinoid composition in the compound eyes of insects. *Exp. Biol.* **47**, 95-103.
Snyder, A. W. (1973). Polarization sensitivity of individual retinula cells. *J. Comp. Physiol. A* **83**, 331-360. doi:10.1007/BF00696351
Snyder, A. W., Menzel, R. and Laughlin, S. B. (1973). Structure and function of the fused rhabdom. *J. Comp. Physiol. A* **87**, 99-135. doi:10.1007/BF01352157
Stalleicken, J., Labhart, T. and Mouritsen, H. (2006). Physiological characterization of the compound eye in monarch butterflies with focus on the dorsal rim area. *J. Comp. Physiol. A* **192**, 321-331. doi:10.1007/s00359-005-0073-6
Stavenga, D. G. (2010). On visual pigment templates and the spectral shape of invertebrate rhodopsins and metarhodopsins. *J. Comp. Physiol. A* **196**, 869-878. doi:10.1007/s00359-010-0568-7
Stavenga, D. G. and Arikawa, K. (2011). Photoreceptor spectral sensitivities of the Small White butterfly *Pieris rapae crucivora* interpreted with optical modeling. *J. Comp. Physiol. A* **197**, 373-385. doi:10.1007/s00359-010-0622-5
Stavenga, D. G., Kinoshita, M., Yang, E.-C. and Arikawa, K. (2001). Retinal regionalization and heterogeneity of butterfly eyes. *Naturwissenschaften* **88**, 477-481. doi:10.1007/s001140100268
Stefanescu, C. (2001). The nature of migration in the red admiral butterfly *Vanessa atalanta*: evidence from the population ecology in its southern range. *Ecol. Entomol.* **26**, 525-536. doi:10.1046/j.1365-2311.2001.00347.x
Stefanescu, C., Alarcón, M. and Àvila, A. (2007). Migration of the painted lady butterfly, *Vanessa cardui*, to north-eastern Spain is aided by African wind currents. *J. Anim. Ecol.* **76**, 888-898. doi:10.1111/j.1365-2656.2007.01262.x
Steiner, A., Paul, R. and Gemperlein, R. (1987). Retinal receptor types in *Aglais urticae* and *Pieris brassicae* (Lepidoptera), revealed by analysis of the electroretinogram obtained with Fourier interferometric stimulation (FIS). *J. Comp. Physiol. A* **160**, 247-258. doi:10.1007/BF00609730
Stewart, F. J., Kinoshita, M. and Arikawa, K. (2019). Monopolatic motion vision in the butterfly *Papilio xuthus*. *J. Exp. Biol.* **222**, jeb191957. doi:10.1242/jeb.191957
Urquhart, F. and Urquhart, N. (1978). Autumnal migration routes of the eastern population of the monarch butterfly (*Danaus p. plexippus* L.; Danaidae; Lepidoptera) in North America to the overwintering site in the Neovolcanic Plateau of Mexico. *Can. J. Zool.* **56**, 1759-1764. doi:10.1139/z78-240
Wakakuwa, M., Stavenga, D. G. and Arikawa, K. (2007). Spectral organization of ommatidia in flower-visiting insects. *Photochem. Photobiol.* **83**, 27-34. doi:10.1562/2006-03-03-IR-831
Wehner, R., Bernard, G. D. and Geiger, E. (1975). Twisted and non-twisted rhabdoms and their significance for polarization detection in the bee. *J. Comp. Physiol. A* **104**, 225-245. doi:10.1007/BF01379050
Yu, H.-Y. (2011). Detection of the long distance movement of the Chestnut Tiger (*Parantica sita niphonica*, Moore) based upon the evidence of population genetic structure. In *Institute of Entomology*, vol. Master's thesis, pp. 56. Taiwan: National Taiwan University.
Zaccardi, G., Kelber, A., Sison-Mangus, M. P. and Briscoe, A. D. (2006). Color discrimination in the red range with only one long-wavelength sensitive opsin. *J. Exp. Biol.* **209**, 1944-1955. doi:10.1242/jeb.02207